Metal ions confinement defines the architecture of G-quartet, G-quadruplex fibrils and their assembly into nematic tactoids

Xiaoyang Li[a,b,c], Antoni Sánchez-Ferrer[c], Massimo Bagnani[c], Jozef Adamcik[c], Paride Azzari[c], Jingcheng Hao[a,b,1], Aixin Song[a,b], Hongguo Liu[a,b], and Raffaele Mezzenga[c,d,1]

[a]Key Laboratory of Colloid and Interface Chemistry, Shandong University, Jinan, Shandong 250100, China; [b]State Key Laboratory of Crystal Materials, Shandong University, Jinan, Shandong 250100, China; [c]Department of Health Sciences and Technology, ETH Zürich, 8092 Zürich, Switzerland; and [d]Department of Materials, ETH Zürich, 8093 Zürich, Switzerland

Edited by Michael L. Klein, Temple University, Philadelphia, PA, and approved March 18, 2020 (received for review November 11, 2019)

G-quadruplex, assembled from a square array of guanine (G) molecules, is an important structure with crucial biological roles in vivo but also a versatile template for ordered functional materials. Although the understanding of G-quadruplex structures is the focus of numerous studies, little is known regarding the control of G-quartet stacking modes and the spontaneous orientation of G-quadruplex fibrils. Here, the effects of different metal ions and their concentrations on stacking modes of G-quartets are elucidated. Monovalent cations (typically K^+) facilitate the formation of G-quadruplex hydrogels with both heteropolar and homopolar stacking modes, showing weak mechanical strength. In contrast, divalent metal ions (Ca^{2+}, Sr^{2+}, and Ba^{2+}) at given concentrations can control G-quartet stacking modes and increase the mechanical rigidity of the resulting hydrogels through ionic bridge effects between divalent ions and borate. We show that for Ca^{2+} and Ba^{2+} at suitable concentrations, the assembly of G-quadruplexes results in the establishment of a mesoscopic chirality of the fibrils with a regular left-handed twist. Finally, we report the discovery of nematic tactoids self-assembled from G-quadruplex fibrils characterized by homeotropic fibril alignment with respect to the interface. We use the Frank–Oseen elastic energy and the Rapini–Papoular anisotropic surface energy to rationalize two different configurations of the tactoids. These results deepen our understanding of G-quadruplex structures and G-quadruplex fibrils, paving the way for their use in self-assembly and biomaterials.

G-quadruplex | metal ions | stacking mode | twisted fibrils | tactoids

In the last few decades, the self-assembly of nucleic acids has significantly expanded the library of supramolecular structures (1–3). Guanine (G)-rich DNA, which could form G-quadruplex DNA, is widely studied because of its relevance with the activity of telomerase in vivo (4, 5). The self-assembly of the small-molecule guanine also has important implications in biology, materials science, nanotechnology, and supramolecular chemistry due to its inherent biocompatibility and biodegradability (6–8). Besides the biological significance, the alternated perpendicular orientation between its hydrogen bonding acceptor and donor moieties endows guanine with the ability to build various ordered architectures, such as G-ribbon and G-quadruplex (9–11). G-ribbon often forms in the absence of metal ions, while G-quadruplex, which consists of the stacking of G-quartets with rotated angle, usually forms in the presence of metal ions (12–14). As promising building blocks, guanine and its derivatives are usually reported as a versatile template to construct functional materials with ordered structure and tunable properties (15–18). Specifically, the stacking modes of G-quartets, as well as the twisted or untwisted fibril morphologies that can be generated from them, might have an effect on the properties and functions of assembled aggregates.

Many works concerning G-quadruplex structures have shown that several factors, such as metal ions, counterions, pH, and concentrations, need to be taken into consideration during its formation (19–26). In particular, metal ions are known to play an important role in the formation of G-quadruplex (27–29). Metal ions with ionic radii in the range of 0.13 to 0.15 nm fit well in the channel of G-quadruplex, and different charges of metal ions define their positions in the G-quadruplex (30). Monovalent metal ions usually bind between every two adjacent G-quartets, while divalent ions cannot appear in succession between G-quartets due to their strong electrostatic repulsion and therefore commonly stay in alternate layers (*SI Appendix*, Fig. S1) (13, 26, 27, 31, 32). Despite great progress in understanding G-quadruplex structures, few works tackled the factors affecting G-quartet stacking mode. At larger length scales, lyotropic cholesteric and hexagonal chromonic mesophases have been reported in G-quadruplex systems (11, 33, 34); however, very little is known and understood about the spontaneous orientation of G-quadruplex fibrils at the microscale level.

In order to shed light on G-quadruplex structures, we chose four metal ions (a monovalent metal ion, K^+, and three divalent metal ions, Ca^{2+}, Sr^{2+}, and Ba^{2+}) to elucidate the factors

Significance

Nucleic acids, essential in living matter, have developed rapidly in nanotechnology due to their biocompatibility and biodegradability. Among these, G-quadruplex, assembled from guanine, bears prime significance due to its implication in the inhibition of telomerase activity in vivo. Furthermore, its unique structure serves as a versatile template for complex architectures used in applications ranging from ion channel to tissue engineering. This work sheds light on the factors affecting the G-quartet stacking mode and their implications on the structure–property relationship in G-quadruplex systems. These results advance our understanding of G-quadruplex structures at different length-scale levels, expanding their scope to chiral fibrils and filamentous liquid crystals, and introducing an adaptable building block in supramolecular soft condensed matter.

Author contributions: X.L., J.H., and R.M. designed research; X.L., A.S.-F., M.B., J.A., P.A., A.S., H.L., and R.M. performed research; X.L., A.S.-F., M.B., J.A., P.A., J.H., A.S., H.L., and R.M. analyzed data; and X.L., A.S.-F., M.B., J.A., P.A., J.H., A.S., H.L., and R.M. wrote the paper.

The authors declare no competing interest.

This article is a PNAS Direct Submission.

Data deposition: The circular dichroism plots, rheology plots, statistic analysis of atomic force microscopy images, and small-angle X-ray scattering and wide-angle X-ray scattering data generated in this study have been deposited in the Dryad digital repository (https://doi.org/10.5061/dryad.j0zpc86b2).

[1]To whom correspondence may be addressed. Email: jhao@sdu.edu.cn or raffaele.mezzenga@hest.ethz.ch.

This article contains supporting information online at https://www.pnas.org/lookup/suppl/doi:10.1073/pnas.1919777117/-/DCSupplemental.

First published April 21, 2020.

affecting the stacking modes of the G-quartet into G-quadruplex (Fig. 1). G-quadruplex structures were then carefully characterized at different length-scale levels by combing different experimental approaches, including circular dichroism (CD), X-ray scattering, rheology, and atomic force microscopy (AFM) analysis. Divalent metal ions (Ca^{2+}, Sr^{2+}, and Ba^{2+}) at certain concentrations induce G-quartets to adopt the same stacking mode through ionic bridge effect, different from G-quadruplex structures induced by monovalent K^+ ions with both heteropolar and homopolar stacking modes. We also show that the rheological properties of G-quadruplex hydrogels are dependent on the ion concentrations and their type.

Finally, we report that in the presence of K^+, the system shows an isotropic–nematic phase transition, where homeotropic nematic tactoids are obtained in a concentration range of guanosine derivative from 38 to 41 mM. These experimental results are supported by theoretical predictions based on the elastic free energy of the system. The ability to control the morphology and the self-assembly of G-quadruplex fibrils into biological liquid crystalline structures can be used for applications in biotechnology and biomedical science (35). Additionally, the spontaneous formation of nematic tactoids at the microscopic level, along with the AFM analysis on the fibril mesoscopic morphologies, give insights into the G-quadruplex fibrils and their self-assembly across different length scales, making them robust building blocks in soft matter.

Results

The Confinement of G-Quartet Stacking Mode. A guanosine derivative in borate ester form (GB) is prepared by the reaction of guanosine (G), phenylboronic acid (PBA), and sodium hydroxide (with a molar ratio of 1:1:1, 50 mM) in water (Fig. 1*A*), which was confirmed by ^{11}B NMR experiments (*SI Appendix*, Fig. S2). In the presence of suitable metal ions, GB could self-assemble into G-quadruplex gels. Since dynamic borate ester can impart injectable and thixotropic properties, many analogous GB gels have been prepared with wide applications such as three-dimensional (3D) printing, drug delivery, catalysis, and electrochemical sensing (36–45). Inspired by their excellent biomaterial and biomedical applications, we investigated the effects of the monovalent ion K^+, and the three divalent ions Ca^{2+}, Sr^{2+}, and Ba^{2+} on the stacking modes of G-quartets.

CD spectroscopy, sensitive to molecular chirality, can be used to detect the formation of G-quadruplex, as well as the stacking orientation of G-quartets (46, 47). CD spectrum of GB aqueous solution does not show G-quadruplex signals in the presence of

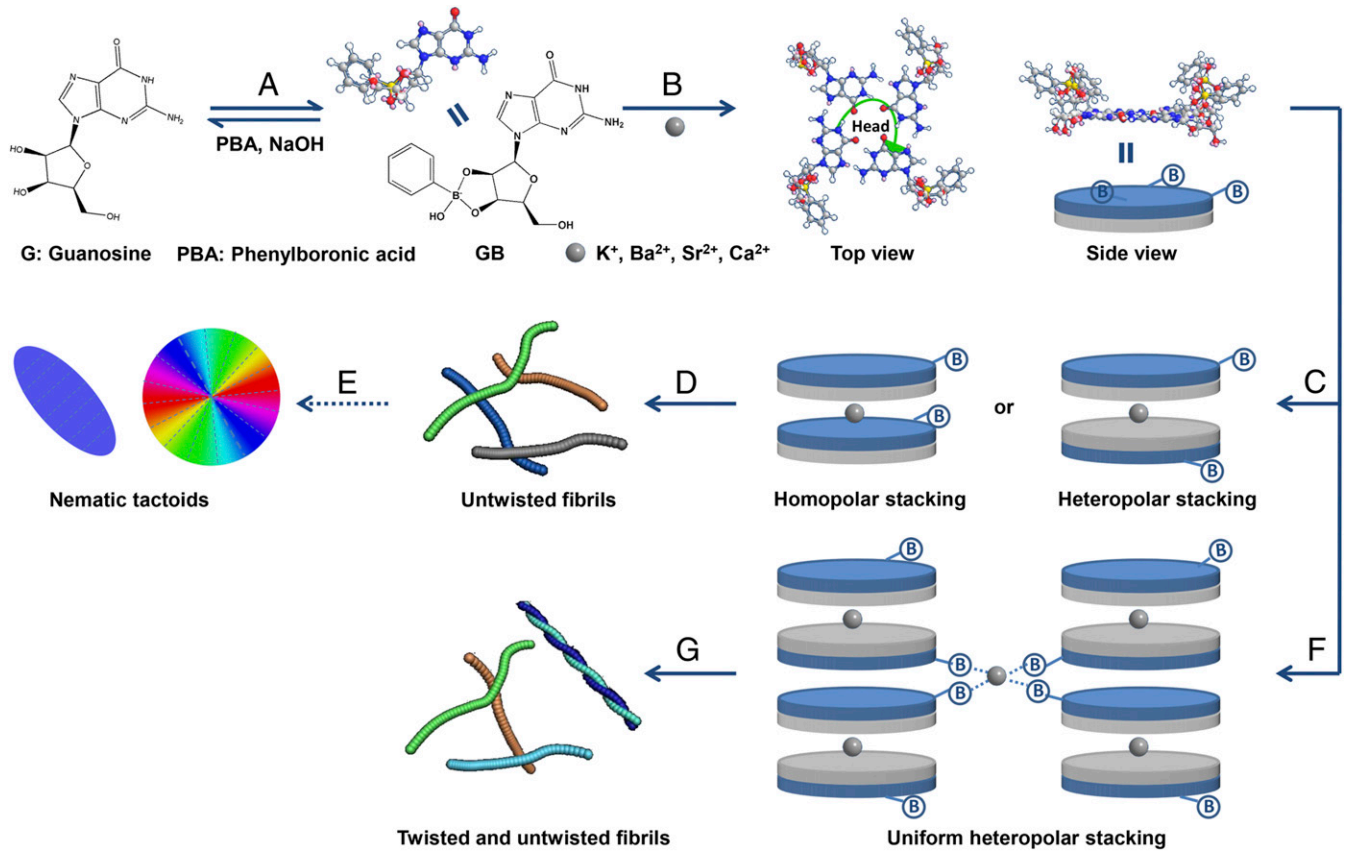

Fig. 1. Schematic representation of the self-assembly of guanosine derivative at different scale levels: (*A*) guanosine derivative in a borate form (GB) was prepared by the reaction of guanosine (G), phenylboronic acid (PBA), and sodium hydroxide in water; (*B*) different metal ions at different concentrations were added to induce the self-assembly of GB into G-quartet; (*C*) for Sr^{2+} and Ba^{2+} at lower concentrations, and K^+ ions, G-quartets stack by both heteropolar and homopolar modes, (*D*) forming untwisted fibrils; (*E*) in the case of GB-K^+ fibrils, nematic tactoids formed when the concentration of GB was in the range of 38 to 41 mM; (*F*) for Sr^{2+} and Ba^{2+} at higher concentrations and for Ca^{2+} ions, G-quartets all adopt the heteropolar stacking mode, (*G*) forming left-handed twisted fibrils in some cases. For a G-quartet, when the rotation direction from hydrogen bonding donors to acceptors is clockwise, this side is defined as the head of G-quartet, and the reverse side with counterclockwise rotation as the tail (46). The head face is shown in blue and the tail in gray. For homopolar stacking, the head of one G-quartet faces the tail of the adjacent one, leading to the same polarity of stacked G-quartets. When the head (tail) of one G-quartet faces the head (tail) of the adjacent one, the stacked G-quartets show opposite polarity, following heteropolar stacking (35). Since the molar ratio of GB to G is about 3 in GB solution analyzed from ^{11}B NMR (*SI Appendix*, Fig. S2), one G-quartet has four guanine parts and also three borate parts. For simplicity, only one borate part is shown in the model. Note: B represents the borate group pointing out to the water media.

Na^+ ions, which are introduced in the preparation process (*SI Appendix*, Fig. S3), and no aggregates are visible from the AFM observation, suggesting that Na^+ ions alone cannot induce G-quadruplex. However, in the presence of monovalent cation, K^+, or divalent cations, Ca^{2+}, Sr^{2+}, and Ba^{2+}, characteristic signals of G-quadruplex can be found in the CD spectra, as shown in Fig. 2*A*. Specifically, there are two main characteristic types of CD signals. One is the signal of G-quadruplex characterized by both homopolar and heteropolar stacking modes, and it shows two sets of CD peaks at ~240 and 260 nm, and ~278 and 300 nm. The other signal is characteristic of the G-quadruplex structure with uniform heteropolar stacking mode, and it shows only one set of peaks at ~278 and 300 nm. According to CD results in Fig. 2*A*, it is confirmed that K^+, Ca^{2+}, Sr^{2+}, and Ba^{2+} ions promote the formation of G-quadruplex but with different stacking modes.

For GB-Sr^{2+} and GB-Ba^{2+} samples, CD signals change drastically with ion concentrations, suggesting that the stacking modes of G-quartet have a transition from the coexistence of heteropolar and homopolar stacking to only heteropolar stacking (Fig. 2*A*). Divalent metal ions usually stay in alternate layer of G-quartets due to the strong electrostatic repulsion between divalent metal ions (*SI Appendix*, Fig. S1), corresponding to a molar ratio of 1:8 between divalent metal ion and GB (13, 27, 31). When the ratio is above 1:8, the channels of G-quadruplex are saturated by Sr^{2+} or Ba^{2+} ions. Excess ions stay at the periphery of G-quadruplex and combine with borate parts (B) at adjacent G-quartets by the ionic bridge effect, causing the confinement of G-quartet stacking modes. When the ratio is above 1:4, that is, the ratio between excess divalent ions (at the periphery of G-quadruplex) and GB is above 1:8, there is one divalent metal ion between every two layers combining with borate parts, confining all G-quartets to a uniform heteropolar stacking mode (Fig. 1*F*). This is consistent with the transition point of CD signals (14:50 ≈ 1:4). This suggests that the transition of CD signals occurs only when all G-quartets adopt the same stacking mode.

For GB-K^+ samples, CD signals show G-quadruplex structures with both heteropolar and homopolar stacking (Fig. 1*A*), independently of ion concentration since there is no ionic bridge effect between excess monovalent K^+ ion and borate. The G-quadruplex structures induced by Ca^{2+} ions only show CD signals characteristic of heteropolar stacking mode for all of the ion concentrations investigated (Fig. 1*A*), similar to GB-Sr^{2+} and GB-Ba^{2+} samples at higher ions concentrations. The confinement of G-quartet stacking modes at lower Ca^{2+} concentrations suggests that there is already an ionic bridge effect between Ca^{2+} ions and borate. Due to a smaller octa-coordinate ionic radius compared to Sr^{2+} and Ba^{2+} (0.112, 0.126, and 0.142 nm for Ca^{2+}, Sr^{2+}, and Ba^{2+}, respectively), Ca^{2+} ions possess relatively weaker binding affinity with eight carbonyl oxygen atoms in the channel of G-quadruplex (27). Therefore, the binding affinity of Ca^{2+} ions with eight carbonyl oxygen atoms in the channel might be similar to that with borate at the periphery of G-quadruplex.

To further verify the formation of G-quadruplex structures, small-angle X-ray scattering (SAXS) and wide-angle X-ray scattering (WAXS) measurements were performed (*SI Appendix*, Figs. S4 and S5). A core-two-shells cylinder form factor P(q) model was adopted in order to extract the core radius and its polydispersity, and both the inner and outer shell thickness (48, 49). In this model, the metal ions make up the core of the fibrils, while the aromatic nucleobases of the G-quartets make up the inner shell, and the attached sugar residues and borate moiety make up the outer shell (Fig. 2*B*). SAXS fitting results show a

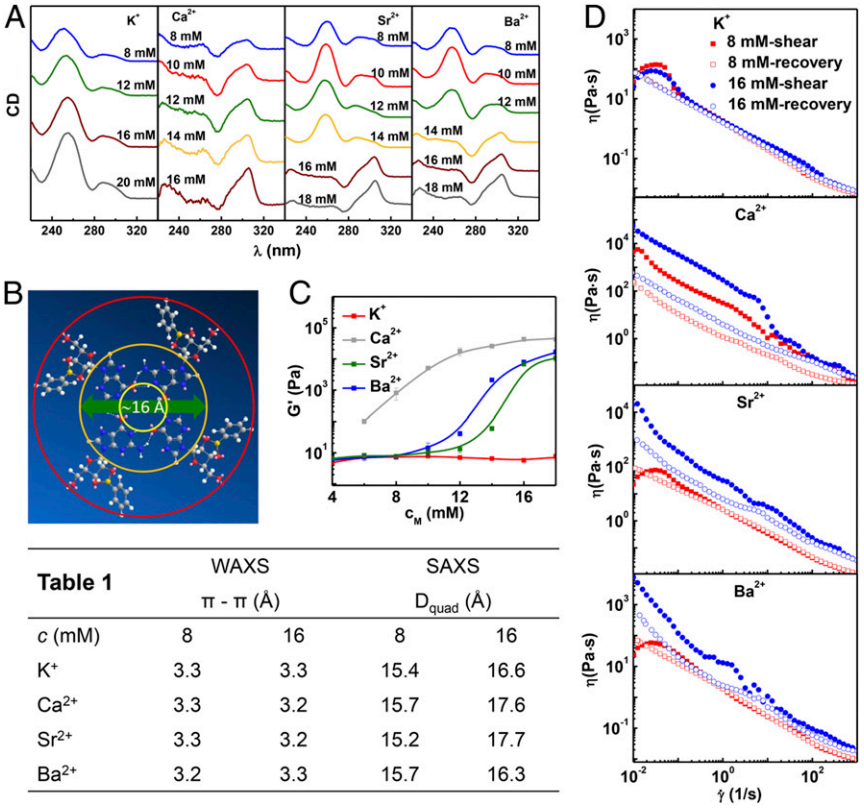

Table 1

	WAXS		SAXS	
	π - π (Å)		D_{quad} (Å)	
c (mM)	8	16	8	16
K^+	3.3	3.3	15.4	16.6
Ca^{2+}	3.3	3.2	15.7	17.6
Sr^{2+}	3.3	3.2	15.2	17.7
Ba^{2+}	3.2	3.3	15.7	16.3

Fig. 2. Characterization of G-quadruplex structures in the presence of monovalent ions (K^+) and divalent ions (Ca^{2+}, Sr^{2+}, and Ba^{2+}). (*A*) CD spectra of ions-induced G-quadruplex with different stacking modes. (*B*) Molecular model of the G-quartet structure, showing the diameter of G-quartet core. (*C*) The elastic modulus (G′) of ions-induced G-quadruplex hydrogels, extracted from frequency-dependent oscillatory shear experiment, as a function of ion concentration. (*D*) Viscosity of ions-induced hydrogels as a function of shear rate by shear-recovery experiment. *Table 1* shows the π–π stacking distance of G-quartets and the diameter of G-quartets provided by the WAXS and SAXS analysis, respectively. The concentration of GB is 50 mM.

core radius of ca. 3 Å, and a total shell thickness of 11.1 to 12.7 Å (*SI Appendix*, Fig. S4), which is consistent with a molecular model of the G-quartets (Fig. 2*B*). From this model, the radius of the metal-occupied core and the G-quartet shell is ca. 8.0 Å and the outer sugar-borate motif is ca. 5.7 Å, resulting into a quadruplex and cylindrical diameter of ca. 16 and 28 Å, respectively (*SI Appendix*, Table S1). WAXS intensity profiles on the freeze-dried samples show a characteristic peak around 3.3 Å (Fig. 2, *Table 1*), which corresponds to the π–π stacking distance of G-quartets (50–52). Moreover, the freeze-dried fibrils show a columnar oblique packing of the cylinders with lattice parameters of ca. $a = 22$ Å and $b = 13$ Å, and $\gamma = 100°$, which fits well with the interdigitating model of the G-quadruplex fibrils (*SI Appendix*, Table S2). Therefore, SAXS and WAXS results confirm a G-columnar structure formed by the stacking of G-quartets, which is consistent with CD results.

As shown in *SI Appendix*, Fig. S4, the SAXS intensity profiles of these hydrogels show a deviation from the experimental data at low q values because of the interactions between the G-quadruplex fibrils, which is reflected by the presence of a structure factor S(q). Thus, by dividing the SAXS intensity profile I(q) by the fitted form factor P(q) from the model, the structure factor S(q) could be obtained showing a maximum at ca. 11 to 14 nm, which could be attributed to the most probable distance between clusters of G-quadruplex fibrils (*SI Appendix*, Fig. S6).

Rheological Properties of G-Quadruplex Hydrogels. It is expected that G-quadruplex structures characterized by different stacking modes might be related to different macroscopic mechanical properties at the gel level. To verify this hypothesis, we investigated the rheological properties of G-quadruplex hydrogels (Fig. 2 *C* and *D* and *SI Appendix*, Fig. S7). The elastic modulus G′ could be used to evaluate the mechanical rigidity. As shown in Fig. 2*C*, the elastic modulus of GB-K^+ hydrogels is very low and is almost independent of ion concentrations. It has been reported that the presence of K^+ could promote Na^+ to bind with G-quadruplex (53). With the addition of K^+ ions, Na^+ ions are involved in the construction of G-quadruplex together with K^+ ions, forming G-quadruplex hydrogels. The added K^+ ions gradually replace Na^+ ions in the channel of G-quadruplex rather than construct new aggregates, leaving unaffected the rigidity of the fibrous network with increasing ion concentration. Moreover, the low elasticity implies the absence of strong bonding between fibrils. This is because GB-K^+ hydrogels are only induced by the simple entanglement of the fibrils (54).

For GB-Sr^{2+} and GB-Ba^{2+} hydrogels, the mechanical rigidity does not increase at lower concentrations, behaving like GB-K^+ hydrogels, and begins to increase from 8 mM. According to the discussion in CD results, at lower concentrations, Sr^{2+} and Ba^{2+} ions go into the channel to construct G-quadruplex. In this case, gels are induced by simple entanglement of fibrils, causing a low elasticity. At higher concentrations, excess Sr^{2+} or Ba^{2+} ions at the periphery of G-quadruplex structures combine with borate at two G-quadruplex fibrils by ionic bridge effect (Fig. 1*F*), causing the physical cross-linking of fibrils and thus an increase of mechanical rigidity.

For GB-Ca^{2+} hydrogels, the shear modulus increases gradually with increasing ion concentration until a plateau is reached above 12 mM. The increase of shear modulus suggests the existence of ionic bridge effect from a low concentration of Ca^{2+} ions, consistent with the conclusion in CD results. The confinement of G-quartet stacking mode and the increase of rigidity are both due to the ionic bridge effect of divalent metal ions with borate at the periphery of G-quadruplex structure: The combination with borate at adjacent G-quartets causes the confinement of stacking mode; meanwhile, the combination with borate at two G-quadruplex fibrils causes the cross-linking of fibrils and therefore an increase of mechanical rigidity (Fig. 1*F*). There have been works reporting the cross-linking of G-quadruplex fibers through multivalent cations such as Mg^{2+}, Ca^{2+}, and Fe^{3+} (38, 55), but little is known about the role of divalent cations in controlling the stacking mode of G-quartet.

In order to demonstrate the above hypotheses, we studied the interaction between fibrils by the shear-recovery experiment. As shown in Fig. 2*D*, there are two types of shear-recovery curves. For hydrogels formed with K^+ at 8 and 16 mM, Sr^{2+} and Ba^{2+} at 8 mM, shear curves are overlapped with recovery curves. The quick recovery implies a simple entanglement between fibrils, proving that there is no ionic bridge effect between metal ions and borate in systems with K^+ ions, or with Sr^{2+} and Ba^{2+} ions at lower concentrations. On the other hand, for hydrogels formed with Sr^{2+} and Ba^{2+} at 16 mM, Ca^{2+} at 8 and 16 mM, recovery curves are lower than shear curves, suggesting a delay of the complete recovery of fibril networks. This implies that fibrils are both cross-linked and entangling, demonstrating the presence of ionic bridge effect in systems with Ba^{2+} and Sr^{2+} ions at higher concentrations, and with Ca^{2+} ions.

We performed continuous strain step tests to confirm the self-recovery property of hydrogels. Strain sweeps were first carried out to determine the linear viscoelastic region (*SI Appendix*, Fig. S8). A low applied strain and a high strain were chosen for the recovery and destruction of hydrogels, respectively, in continuous step strain tests ($\gamma = 1\%$ and 500% for hydrogels formed with K^+ at 8 and 16 mM, Sr^{2+} and Ba^{2+} at 8 mM; $\gamma = 0.1\%$ and 200% for hydrogels formed with Ca^{2+} at 8 and 16 mM, Sr^{2+} and Ba^{2+} at 16 mM). As shown in *SI Appendix*, Fig. S9, when hydrogels were subjected to high step strains, a transition from gel to sol occurred ($G' < G''$); when low step strains were imposed, hydrogels could reform but with different recovery ratios. Hydrogels formed with K^+ at 8 and 16 mM, Sr^{2+} and Ba^{2+} at 8 mM, showed a rapid recovery within 60 s and a recovery ratio of more than 90% over four cycles (*SI Appendix*, Table S3), suggesting a good self-recovery ability. In contrast, hydrogels formed with Ca^{2+} at 8 and 16 mM, Sr^{2+} and Ba^{2+} at 16 mM, showed relatively weaker ability for self-recovery with recovery ratios of 32%, 20%, 60%, and 57%, respectively (*SI Appendix*, Table S3). This result is consistent with the data in shear-recovery experiment.

Fibril Morphology. In order to further characterize the structure and the morphology of the supramolecular aggregates, AFM imaging was performed on aliquots of the hydrogels formed in the presence of these four metal ions at two different concentrations, 8 and 16 mM (Fig. 3*A*). The typical persistence length (λ) of these fibrils is hundreds (Fig. 3*B*) to thousands (*SI Appendix*, Fig. S10) of nanometers, thus at least two orders of magnitude larger than the Debye length. Therefore, rigidity is expected to be rather insensitive to ionic strength, and we expect a behavior very different from classical polyelectrolytes or charged worm-like micelles, which increase flexibility with increasing salt content (56, 57). On the contrary, we observe that the height distribution of all fibrils with various salt series shifts toward higher heights when increasing ion concentration from 8 to 16 mM (Fig. 3*F*), with the distributions becoming bimodal in all cases of K^+, Ca^{2+}, Sr^{2+}, and Ba^{2+}, including the cases where the initial distribution of height at 8 mM is clearly monomodal (K^+ and Ba^{2+}). A systematic increase of the average height $\langle h \rangle$ is also found in all systems. As the persistence length for semiflexible polymers is known to scale as $\lambda \sim \langle h \rangle^4$ (58), it is concluded that the persistence length of fibrils increases with ion concentration, following a behavior opposite to traditional polyelectrolytes. This behavior is a fingerprint of the supramolecular coordination between the guanine molecules and the cations in solution.

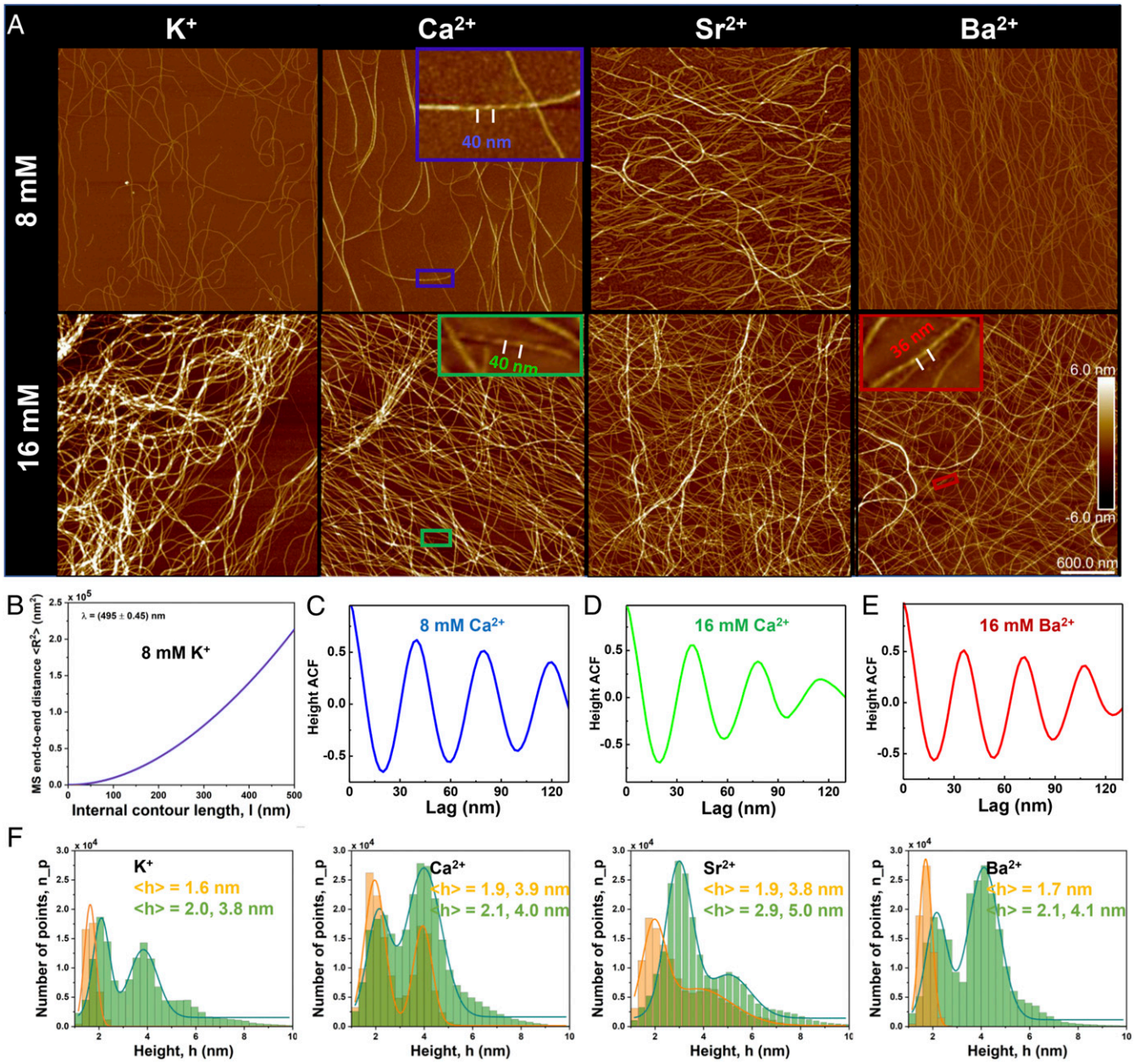

Fig. 3. The characterization of fibril morphology formed by K^+, Ca^{2+}, Sr^{2+}, and Ba^{2+} at 8 and 16 mM. (*A*) AFM images of the fibrils morphology. (All images are with the same scale bar: 600 nm.) (*B*) Persistence length estimation for fibrils formed with 8 mM K^+ by the 2D worm-like chain model. The persistence length is about 500 nm. Height profiles showing the pitch of left-handed twisted fibrils formed by Ca^{2+} at 8 mM (*C*) and 16 mM (*D*), and Ba^{2+} at 16 mM (*E*). (*F*) The height distribution of fibrils formed with four cations at 8 mM (orange) and 16 mM (green). The concentration of **GB** is 50 mM. The statistical analysis is performed by FiberApp (70).

For the thin fibrils formed with K^+ and Ba^{2+} at 8 mM, the average height is about 1.6 nm (Fig. 3*F*), which is in agreement with the diameter of the G-quartet core obtained by SAXS experiments (if the sugar moiety falls apart upon freeze-drying), confirming that these thin fibrils are composed of stacked G-quartets and are individual G-quadruplex without lateral pairing. Interestingly, in the samples formed by 8 and 16 mM Ca^{2+}, and 16 mM Ba^{2+}, left-handed twisted fibrils could be observed (Fig. 3*A* and *SI Appendix*, Fig. S11). The height profiles give the average pitches of the twisted fibrils, which are about 40, 40, and 36 nm for samples formed by 8 and 16 mM Ca^{2+}, and 16 mM Ba^{2+}, respectively (Fig. 3 *C*–*E*), disclosing a regular mesoscopic chirality in metal-induced G-quadruplex fibrils. In the samples with uniform heteropolar stacking mode left-handed twisted fibrils occasionally were observed, while in the samples with both heteropolar and homopolar stacking modes no twisted fibrils are formed. Therefore, AFM observations reveal a rich polymorphism on fibrils (twisted and untwisted) dependent on types and concentrations of metal ions.

Nematic Tactoids with Negative Anchoring Strength. Liquid crystals, with their self-assembling properties, are a subject of extensive academic research and are used in various applications, such as displays, lasers, and biochemical sensors (59). Liquid crystalline systems based on biological semiflexible polymers are attracting increasing attention from the research community, for their

potential applications in biotechnology and biomedical sciences (35). Examples range from DNA and cellulose to amyloid fibrils (59–61).

Colloidal rod-like particles can undergo to spontaneous liquid crystalline phase transitions when dispersed at high enough concentrations (62). This liquid–liquid phase separation is characterized by the coexistence of a continuous isotropic phase, where dispersed rod-like particles are randomly oriented, and a more concentrated nematic phase, in which mesogens spontaneously assume orientational order (63). These dispersed domains, also known as tactoids, appear birefringent under cross-polarized microscope and can assume a broad range of configurations depending on the system properties (64). In particular, the shape and the orientational director field configuration of a tactoid depend on a subtle interplay of anisotropic interfacial and bulk energies and is a vibrant area of research (65–67).

Since G-quadruplex is of vital importance in both biology and supramolecular chemistry, it is of great significance to gain insight into the nature and geometry of the interactions of G-quadruplex fibrils. Cholesteric and hexagonal mesophases have been observed in G-quadruplex systems, whose basic structure is a chiral columnar aggregate based on the stacking of G-quartets (34, 68). However, to the best of our knowledge, no studies have reported tactoids composed of G-quadruplex fibrils. Considering that using K^+ ions G-quadruplex structures could be effectively induced without ionic bridge effects interfering with liquid crystalline order, G-quadruplex fibrils were prepared by the reaction of G, PBA, and KOH (*SI Appendix*, Figs. S12 and S13). Based on the formation of G-quadruplex fibrils, a phase diagram of the ensued liquid crystalline mesophases was established by varying the concentrations of GB and fixing the reaction molar ratio of G, PBA, and KOH at 1:1:1 (*SI Appendix*, Fig. S14). Hydrogels with the concentration of GB below 38 mM were isotropic and showed no birefringence under polarized light. At concentrations above 41 mM, however, they appeared completely birefringent, implying the formation of a nematic phase.

Between these two critical concentrations, the system shows a biphasic behavior, characterized by the formation of liquid-crystalline droplets as expected in the coexistence of the isotropic and nematic phases (*SI Appendix*, Fig. S15). LC PolScope imaging was used to evaluate the director field configuration of the nematic domains: Two different configurations of tactoids were observed, one characterized by a homogeneous nematic director field (Fig. 4 *A–C*) and one with a radial nematic configuration (Fig. 4 *D–F*). In both cases, LC PolScope analysis revealed that the nematic director field is perpendicular to the interface, indicating homeotropic alignment for both configurations (Fig. 4) (67).

The two different configurations were rationalized using the Frank–Oseen elastic energy, coupled with the Rapini–Papoular anisotropic surface energy (67):

$$F = K\int \|\nabla n\|^2 dV + \gamma\int \left(1 + \omega \cos^2\theta\right) dS.$$

The first term describes the curvature of the nematic field n, and it is proportional to the elastic constant K. The second term, proportional to the surface tension γ, depends on the angle θ formed by the nematic field with the normal of the surface of the tactoids. The parameter ω is called anchoring and quantifies the strength of the anisotropy of the surface energy. In our case, homeotropic alignment implies negative anchoring strength.

In the homogeneous tactoids, the elastic energy term dominates, and the resulting shape follows the Wulff construction (64, 66). According to this model, the droplet shape is oblate (i.e., lenticular), with rotational symmetry along the minor axis (69). These tactoids are characterized by an elongated shape with aspect ratio d/D (D, major axis, and d, minor axis) equal to 0.50 ± 0.05, independent of the volume of the tactoid, varying in the range of 10^2 to 10^5 μm^3 (*SI Appendix*, Fig. S16). The tactoids tip angle is measured to be $120° \pm 3°$ (*SI Appendix*, Fig. S17). From the aspect ratio, we estimated an anchoring strength of $\omega = -0.5$.

In the radial nematic tactoids, the surface energy prevails, forcing the droplet to be spherical with homeotropic alignment. The radial nematic tactoids are nearly spherical and characterized by an aspect ratio equal to 1, which is independent of the volume (*SI Appendix*, Fig. S16).

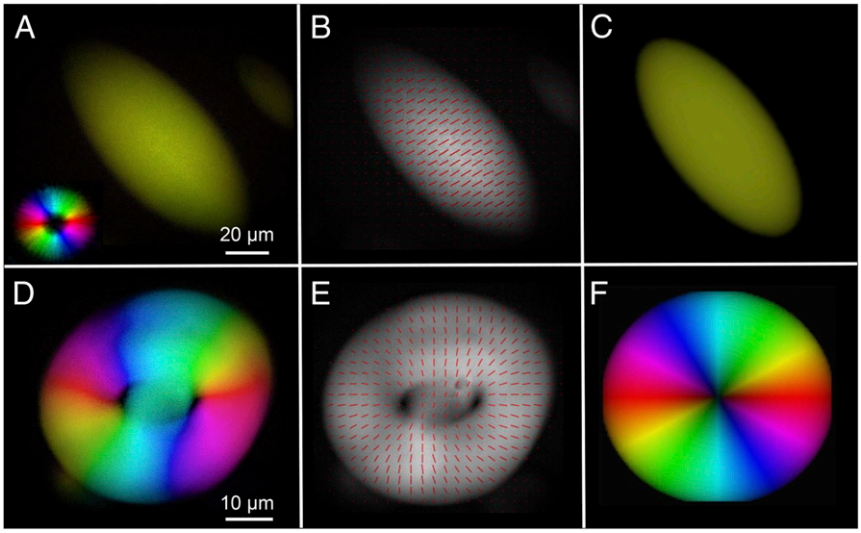

Fig. 4. Liquid-crystalline tactoids: microscopy images of homogeneous nematic tactoids, showing director field always perpendicular to the long axis of the tactoid visualized with LC PolScope color maps microscope (*A*), in grayscale with corresponding orientation lines in *B*, and corresponding theoretical simulation in *C*; radial nematic tactoids with director field perpendicular to the interface shown as color map PolScope image, grayscale and simulation in *D*, *E*, and *F*, respectively. The two dark points at the center of the tactoid shown in *D* and *E* are known as defects and are caused by the spherical confinement. As previously reported, the theoretical model does not predict defects (65). In the color mapped PolScope images, the director field orientation is represented by different colors as in the legend at bottom left of *A*. The concentrations of G, PBA, and KOH are all 40 mM.

Discussion

In this work, we investigated the effect of metal ions on G-quartet stacking modes by combining complementary experimental approaches probing different length scales. In particular, CD, SAXS, and WAXS analysis indicated the formation of G-quadruplex structures promoted by K^+, Ca^{2+}, Sr^{2+}, and Ba^{2+}. Additionally, CD revealed different G-quartet stacking modes depending on the type of metal ion and their concentration. The G-quadruplex formed in presence of monovalent K^+ is characterized by heteropolar and homopolar stacking modes, independently of ion concentration. In the presence of Sr^{2+} and Ba^{2+} ions, G-quartet stacking mode shows an ion concentration-induced transition from the coexistence of heteropolar and homopolar stacking to only heteropolar stacking, suggesting that excess Sr^{2+} and Ba^{2+} ions confine the stacking mode. G-quadruplex promoted by Ca^{2+} shows only heteropolar stacking mode, independently of ion concentrations. Interestingly, the effect of metal ion plays a key role in the establishment of a mesoscopic chirality in the G-quadruplex fibrils, leading to a left-handed regular twist in the case of Ca^{2+} and Ba^{2+} ions intercalated via uniform G-quartet stacking mode.

Rheological experiments showed that different G-quartet stacking modes translate into different rheological properties: While G-quadruplex hydrogels with both heteropolar and homopolar stacking modes show a weak mechanical rigidity, samples with uniform heteropolar stacking have a stronger mechanical rigidity. Increasing the K^+ ion concentration does not affect the weak stiffness of GB-K^+ hydrogels. For GB-Sr^{2+} and GB-Ba^{2+} hydrogels, the shear modulus is invariant at low ions concentrations, but starts to increase above a threshold, where G-quadruplex becomes saturated by divalent metal ions leading to supramolecular bridges among different G-quadruplex fibrils. The concentration of Ca^{2+} ions has a strong influence on the rheological properties of the gels, making them the stiffest gel. These results suggest that ionic bridges of divalent metal ions at the periphery of G-quadruplex are the main factor increasing the rigidity of gels beyond that achievable by pure fibril entanglements. According to this scenario, excess divalent metal ions combine with borate at adjacent G-quartets, leading to the physical cross-linking among distinct G-quadruplex fibrils and therefore increasing their mechanical stiffness.

In the absence of physical cross-links, and for suitable concentrations, G-quadruplex fibrils were found to form liquid-crystalline phases. In the isotropic–nematic coexistence regime of concentration, microscopy analysis revealed the formation of two classes of liquid-crystal tactoids nucleating from an isotropic continuous phase: homogeneous nematic and radial nematic tactoids, both characterized by negative anchoring strength (homeotropic fibril alignment at the interface). This makes G-quadruplex fibrils significantly different from the greatest majority of liquid crystalline filamentous colloids, characterized by a positive anchoring strength and colloidal alignment parallel to the interface. These results advance our understanding of the self-assembly of metal coordinated G-quadruplexes at various length scales, and provide a robust fundamental basis for the rational design of supramolecular building blocks for liquid-crystalline phases with controlled director field distributions. The ability to control the morphology of G-quadruplex fibrils and to tune their self-assembly into liquid-crystalline structures opens to applications and theoretical studies for this class of lyotropic liquid crystals.

Materials and Methods

GB was prepared as a G-assemblies precursor by mixing guanosine, phenylboronic acid, and sodium hydroxide in water and heated to 80 °C for 2 h. In order to obtain hydrogels, four types of salts (KCl, $CaCl_2$, $SrCl_2$, $BaCl_2$) at different concentrations were added to GB aqueous solutions, which were then slowly cooled down to room temperature. The resulted hydrogels were characterized at different length scales by CD, SAXS, WAXS, AFM, and rheology. The liquid-crystalline droplets assembled from G-quadruplex fibrils were prepared by guanosine, phenylboronic acid, and potassium hydroxide (in water) with a molar ratio of 1:1:1. The formed liquid-crystal droplets were characterized by LC Polscope. More information about materials and methods is given in *SI Appendix*.

Data Availability. All data discussed in the paper have been deposited in the Dryad digital repository, https://doi.org/10.5061/dryad.j0zpc86b2. All data will also be made available via direct inquires.

ACKNOWLEDGMENTS. X.L. thanks the China Scholarship Council for financial support. Funds from ETH Zürich (Grant SEED-43 16 1) and the National Natural Science Foundation of China (Grants 21420102006 and ZR2018ZA0547) are gratefully acknowledged.

1. S. M. Douglas *et al.*, Self-assembly of DNA into nanoscale three-dimensional shapes. *Nature* **459**, 414–418 (2009).
2. Y. He *et al.*, Hierarchical self-assembly of DNA into symmetric supramolecular polyhedra. *Nature* **452**, 198–201 (2008).
3. G. M. Peters, J. T. Davis, Supramolecular gels made from nucleobase, nucleoside and nucleotide analogs. *Chem. Soc. Rev.* **45**, 3188–3206 (2016).
4. S. Burge, G. N. Parkinson, P. Hazel, A. K. Todd, S. Neidle, Quadruplex DNA: Sequence, topology and structure. *Nucleic Acids Res.* **34**, 5402–5415 (2006).
5. M. L. Bochman, K. Paeschke, V. A. Zakian, DNA secondary structures: Stability and function of G-quadruplex structures. *Nat. Rev. Genet.* **13**, 770–780 (2012).
6. J. T. Davis, G-quartets 40 years later: From 5′-GMP to molecular biology and supramolecular chemistry. *Angew. Chem. Int. Ed. Engl.* **43**, 668–698 (2004).
7. S. Lena, S. Masiero, S. Pieraccini, G. P. Spada, Guanosine hydrogen-bonded scaffolds: A new way to control the bottom-up realisation of well-defined nanoarchitectures. *Chemistry* **15**, 7792–7806 (2009).
8. J. T. Davis, G. P. Spada, Supramolecular architectures generated by self-assembly of guanosine derivatives. *Chem. Soc. Rev.* **36**, 296–313 (2007).
9. G. Paragi, C. Fonseca Guerra, Cooperativity in the self-assembly of the guanine nucleobase into quartet and ribbon structures on surfaces. *Chemistry* **23**, 3042–3050 (2017).
10. M. El Garah *et al.*, Guanosine-based hydrogen-bonded 2D scaffolds: Metal-free formation of G-quartet and G-ribbon architectures at the solid/liquid interface. *Chem. Commun. (Camb.)* **51**, 11677–11680 (2015).
11. S. Lena *et al.*, Self-assembly of an alkylated guanosine derivative into ordered supramolecular nanoribbons in solution and on solid surfaces. *Chemistry* **13**, 3757–3764 (2007).
12. X. Wang *et al.*, Reversible organogels triggered by dynamic K^+ binding and release. *J. Colloid Interface Sci.* **353**, 412–419 (2011).
13. D. Hu, J. Ren, X. Qu, Metal-mediated fabrication of new functional G-quartet-based supramolecular nanostructure and potential application as controlled drug release system. *Chem. Sci.* **2**, 1356–1361 (2011).
14. A. Ciesielski, S. Lena, S. Masiero, G. P. Spada, P. Samorì, Dynamers at the solid-liquid interface: Controlling the reversible assembly/reassembly process between two highly ordered supramolecular guanine motifs. *Angew. Chem. Int. Ed. Engl.* **49**, 1963–1966 (2010).
15. L. Min *et al.*, Transcription of G-quartet supramolecular aggregates into hierarchical mesoporous silica nanotubes. *Dalton Trans.* **45**, 7912–7920 (2016).
16. P. Singh, V. Venkatesh, N. Nagapradeep, S. Verma, A. Bianco, G-quartet type self-assembly of guanine functionalized single-walled carbon nanotubes. *Nanoscale* **4**, 1972–1974 (2012).
17. G. P. Spada *et al.*, Guanosine-based hydrogen-bonded scaffolds: Controlling the assembly of oligothiophenes. *Adv. Mater.* **20**, 2433–2438 (2008).
18. C. Arnal-Hérault, A. Banu, M. Barboiu, M. Michau, A. van der Lee, Amplification and transcription of the dynamic supramolecular chirality of the guanine quadruplex. *Angew. Chem. Int. Ed. Engl.* **46**, 4268–4272 (2007).
19. L. E. Buerkle, Z. Li, A. M. Jamieson, S. J. Rowan, Tailoring the properties of guanosine-based supramolecular hydrogels. *Langmuir* **25**, 8833–8840 (2009).
20. G. M. Peters *et al.*, A G_4·K^+ hydrogel stabilized by an anion. *J. Am. Chem. Soc.* **136**, 12596–12599 (2014).
21. G. M. Peters, L. P. Skala, J. T. Davis, A molecular chaperone for G4-quartet hydrogels. *J. Am. Chem. Soc.* **138**, 134–139 (2016).
22. S. Lena, P. Neviani, S. Masiero, S. Pieraccini, G. P. Spada, Triggering of guanosine self-assembly by light. *Angew. Chem. Int. Ed. Engl.* **49**, 3657–3660 (2010).
23. I. C. Kwan, R. J. Delley, D. R. Hodgson, G. Wu, Single atom modification leads to enhanced nucleotide self-assembly: The role of cation bridging. *Chem. Commun. (Camb.)* **47**, 3882–3884 (2011).
24. I. Bald *et al.*, Control of self-assembled 2D nanostructures by methylation of guanine. *Small* **7**, 939–949 (2011).
25. D. González-Rodríguez *et al.*, G-quadruplex self-assembly regulated by Coulombic interactions. *Nat. Chem.* **1**, 151–155 (2009).
26. X. Shi, J. C. Fettinger, J. T. Davis, Ion-pair recognition by nucleoside self-assembly: Guanosine hexadecamers bind cations and anions. *Angew. Chem. Int. Ed.* **40**, 2827–2831 (2001).

27. I. C. M. Kwan, Y.-M. She, G. Wu, Nuclear magnetic resonance and mass spectrometry studies of 2′,3′,5′-*o*-triacetylguanosine self-assembly in the presence of alkaline earth metal ions (Ca^{2+}, Sr^{2+}, Ba^{2+}). *Can. J. Chem.* **89**, 835–844 (2011).
28. A. Wong, G. Wu, Selective binding of monovalent cations to the stacking G-quartet structure formed by guanosine 5′-monophosphate: A solid-state NMR study. *J. Am. Chem. Soc.* **125**, 13895–13905 (2003).
29. F. W. Kotch, J. C. Fettinger, J. T. Davis, A lead-filled G-quadruplex: Insight into the G-quartet's selectivity for Pb^{2+} over K^+. *Org. Lett.* **2**, 3277–3280 (2000).
30. B. I. Kankia, L. A. Marky, Folding of the thrombin aptamer into a G-quadruplex with Sr^{2+}: Stability, heat, and hydration. *J. Am. Chem. Soc.* **123**, 10799–10804 (2001).
31. I. C. M. Kwan, Y.-M. She, G. Wu, Trivalent lanthanide metal ions promote formation of stacking G-quartets. *Chem. Commun. (Camb.)* **2007**, 4286–4288 (2007).
32. J. Gu, J. Leszczynski, A remarkable alteration in the bonding pattern: An HF and DFT study of the interactions between the metal cations and the Hoogsteen hydrogen-bonded G-tetrad. *J. Phys. Chem. A* **104**, 6308–6313 (2000).
33. G. Gottarelli, G. Proni, G. P. Spada, The self-assembly and lyotropic mesomorphism of riboguanylic acids (GMP). *Liq. Cryst.* **22**, 563–566 (1997).
34. P. Mariani, C. Mazabard, A. Garbesi, G. P. Spada, A study of the structure of the lyomesophases formed by the dinucleoside phosphate d(GpG). An approach by X-ray diffraction and optical microscopy. *J. Am. Chem. Soc.* **111**, 6369–6373 (1989).
35. G. Nyström, M. Arcari, R. Mezzenga, Confinement-induced liquid crystalline transitions in amyloid fibril cholesteric tactoids. *Nat. Nanotechnol.* **13**, 330–336 (2018).
36. G. M. Peters *et al*., G4-quartet·M^+ borate hydrogels. *J. Am. Chem. Soc.* **137**, 5819–5827 (2015).
37. V. Venkatesh *et al*., Supramolecular photoactivatable anticancer hydrogels. *J. Am. Chem. Soc.* **139**, 5656–5659 (2017).
38. A. Rotaru *et al*., G-quartet hydrogels for effective cell growth applications. *Chem. Commun. (Camb.)* **53**, 12668–12671 (2017).
39. T. Bhattacharyya, Y. P. Kumar, J. Dash, Supramolecular hydrogel inspired from DNA structures mimics peroxidase activity. *ACS Biomater. Sci. Eng.* **3**, 2358–2365 (2017).
40. R. Zhong *et al*., Self-assembly of enzyme-like nanofibrous G-molecular hydrogel for printed flexible electrochemical sensors. *Adv. Mater.* **30**, e1706887 (2018).
41. F. Chen *et al*., General strategy to fabricate strong and tough low-molecular-weight gelator-based supramolecular hydrogels with double network structure. *Chem. Mater.* **30**, 1743–1754 (2018).
42. R. Zhong *et al*., Logic catalytic interconversion of G-molecular hydrogel. *ACS Appl. Mater. Interfaces* **10**, 4512–4518 (2018).
43. A. Biswas, S. Malferrari, D. M. Kalaskar, A. K. Das, Arylboronate esters mediated self-healable and biocompatible dynamic G-quadruplex hydrogels as promising 3D-bioinks. *Chem. Commun. (Camb.)* **54**, 1778–1781 (2018).
44. J. Li *et al*., A multifunctional self-healing G-PyB/KCl hydrogel: Smart conductive, rapid room-temperature phase-selective gelation, and ultrasensitive detection of alpha-fetoprotein. *Chem. Commun. (Camb.)* **55**, 7922–7925 (2019).
45. A. Biswas, S. Maiti, D. M. Kalaskar, A. K. Das, Redox-active dynamic self-supporting thixotropic 3D-printable G-quadruplex hydrogels. *Chem. Asian J.* **13**, 3928–3934 (2018).
46. S. Masiero *et al*., A non-empirical chromophoric interpretation of CD spectra of DNA G-quadruplex structures. *Org. Biomol. Chem.* **8**, 2683–2692 (2010).
47. G. Gottarelli, S. Lena, S. Masiero, S. Pieraccini, G. P. Spada, The use of circular dichroism spectroscopy for studying the chiral molecular self-assembly: An overview. *Chirality* **20**, 471–485 (2008).
48. R. Bomba, W. Kwiatkowski, A. Sánchez-Ferrer, R. Riek, J. Greenwald, Cooperative induction of ordered peptide and fatty acid aggregates. *Biophys. J.* **115**, 2336–2347 (2018).
49. A. Sánchez-Ferrer *et al*., Controlling supramolecular chiral nanostructures by self-assembly of a biomimetic β-sheet-rich amyloidogenic peptide. *ACS Nano* **12**, 9152–9161 (2018).
50. Y. Li *et al*., A G-quadruplex hydrogel via multicomponent self-assembly: Formation and zero-order controlled release. *ACS Appl. Mater. Interfaces* **9**, 13056–13067 (2017).
51. A. Wong, R. Ida, L. Spindler, G. Wu, Disodium guanosine 5′-monophosphate self-associates into nanoscale cylinders at pH 8: A combined diffusion NMR spectroscopy and dynamic light scattering study. *J. Am. Chem. Soc.* **127**, 6990–6998 (2005).
52. R. Belda, E. García-España, G. A. Morris, J. W. Steed, J. A. Aguilar, Guanosine-5′-monophosphate polyamine hybrid hydrogels: Enhanced gel strength probed by z-spectroscopy. *Chemistry* **23**, 7755–7760 (2017).
53. C. Detellier, P. Laszlo, Role of alkali metal and ammonium cations in the self-assembly of the 5′-guanosine monophosphate dianion. *J. Am. Chem. Soc.* **102**, 1135–1141 (1980).
54. Y. Cao, S. Bolisetty, J. Adamcik, R. Mezzenga, Elasticity in physically cross-linked amyloid fibril networks. *Phys. Rev. Lett.* **120**, 158103 (2018).
55. N. Thakur *et al*., Biocompatible Fe^{3+} and Ca^{2+} dual cross-linked G-quadruplex hydrogels as effective drug delivery system for pH-responsive sustained zero-order release of doxorubicin. *ACS Appl. Bio Mater.* **2**, 3300–3311 (2019).
56. M. E. Cates, S. J. Candau, Statics and dynamics of worm-like surfactant micelles. *J. Phys. Condens. Matter* **2**, 6869–6892 (1990).
57. C. Lara, I. Usov, J. Adamcik, R. Mezzenga, Sub-persistence-length complex scaling behavior in lysozyme amyloid fibrils. *Phys. Rev. Lett.* **107**, 238101 (2011).
58. J. Adamcik *et al*., Understanding amyloid aggregation by statistical analysis of atomic force microscopy images. *Nat. Nanotechnol.* **5**, 423–428 (2010).
59. S. J. Woltman, G. D. Jay, G. P. Crawford, Liquid-crystal materials find a new order in biomedical applications. *Nat. Mater.* **6**, 929–938 (2007).
60. G. Nystrom, R. Mezzenga, Liquid crystalline filamentous biological colloids: Analogies and differences. *Curr. Opin. Colloid Interface Sci.* **38**, 30–44 (2018).
61. S. J. Woltman, G. D. Jay, G. P. Crawford, *Liquid Crystals: Frontiers in Biomedical Applications*, (World Scientific, Hackensack, NJ, 2007).
62. L. Tortora *et al*., Self-assembly, condensation, and order in aqueous lyotropic chromonic liquid crystals crowded with additives. *Soft Matter* **6**, 4157–4167 (2010).
63. A. D. Rey, Liquid crystal models of biological materials and processes. *Soft Matter* **6**, 3402–3429 (2010).
64. M. Bagnani, G. Nyström, C. De Michele, R. Mezzenga, Amyloid fibrils length controls shape and structure of nematic and cholesteric tactoids. *ACS Nano* **13**, 591–600 (2019).
65. M. Bagnani, P. Azzari, S. Assenza, R. Mezzenga, Six-fold director field configuration in amyloid nematic and cholesteric phases. *Sci. Rep.* **9**, 12654 (2019).
66. P. Prinsen, P. van der Schoot, Continuous director-field transformation of nematic tactoids. *Eur Phys J E Soft Matter* **13**, 35–41 (2004).
67. P. Prinsen, P. van der Schoot, Shape and director-field transformation of tactoids. *Phys. Rev. E Stat. Nonlin. Soft Matter Phys.* **68**, 021701 (2003).
68. F. C. MacKintosh, J. Käs, P. A. Janmey, Elasticity of semiflexible biopolymer networks. *Phys. Rev. Lett.* **75**, 4425–4428 (1995).
69. R. L. Dobrushin, R. Kotecky, S. B. Shlosman, *Wulff Construction: A Global Shape from Local Interaction* (American Mathematical Society, Providence, RI, 1992).
70. I. Usov, R. Mezzenga, Fiberapp: An open-source software for tracking and analyzing polymers, filaments, biomacromolecules, and fibrous objects. *Macromolecules* **48**, 1269–1280 (2015).